Chinese Chemical Letters 35 (2024) 109413

Contents lists available at ScienceDirect

Chinese Chemical Letters

journal homepage: www.elsevier.com/locate/cclet

Degradation of neonicotinoids with different molecular structures in heterogeneous peroxymonosulfate activation system through different oxidation pathways

Ruonan Guo [a,b], Heng Zhang [a], Changsheng Guo [a], Ningqing Lv [a], Beidou Xi [a,b], Jian Xu [a,*]

[a] State Key Laboratory of Environmental Criteria and Risk Assessment, Chinese Research Academy of Environmental Sciences, Beijing 100012, China
[b] School of Environment, Tsinghua University, Beijing 100084, China

ARTICLE INFO

Article history:
Received 27 August 2023
Revised 4 December 2023
Accepted 19 December 2023
Available online 21 December 2023

Keywords:
Fenton-like processes
Molecular structure
Neonicotinoids
Nonradical oxidation
Degradation pathway

ABSTRACT

The elimination of neonicotinoids (NEOs) from water has been a research priority due to their threats to human health and ecosystems. In this study, we established the heterogeneous peroxymonosulfate (PMS) activation system using manganese catalyst (Mn NC) and cobalt catalyst (Co NC) to trigger the nonradical oxidation and synergistic oxidation pathway, respectively to remove NEOs. The results showed that the nonradical oxidation system exhibited superior NEOs degradation capability. The composition of organic pollutants in wastewater significantly impacted subsequent degradation processes. The charge distribution and reaction sites of various NEOs were analyzed using density functional theory (DFT) calculations, and it demonstrated the electron distribution and activity of NEOs were significantly influenced by the type and number of substituents. Nitro group ($-NO_2$) and cyanide group ($-C\equiv N$) were identified as strong electron-withdrawing groups and prone to be attacked by negatively charged radicals. The transformation of NEOs was analyzed, and result showed that the C and N sites adjacent to the nitro group and cyanide group were more susceptible to oxidation attacks. S and N atoms, which possess strong electronegativity and high electron cloud density, were identified as key active sites in the degradation pathway. The outcomes of this study provide valuable guidance for the oriented regulation of oxidation pathways towards efficient removal of NEOs in water.

Neonicotinoids (NEOs) are a new class of neurotoxic insecticides that disrupt the nervous system and biological processes of insects. They are typically derived from modifications of the basic nicotine skeleton, involving substituents or functional groups. Since 1980s, NEOs have replaced traditional insecticides and become widely used insecticides in modern crop protection [1]. However, only 5% of NEOs are utilized by plants after application, with remaining entering the natural environment [2]. Due to their physicochemical properties and widespread usage, NEOs may rapidly migrate from their initial application sites to water environment. The presence of NEOs has been detected in various water bodies around the world, including agricultural areas as well as natural water bodies distant from agriculture [3–6]. While selective toxicity enhances safety for nontarget vertebrate organisms, both *in vitro* and *in vivo* studies have demonstrated that exposure to NEOs can induce endocrine-disrupting effects [7], neurotoxicity [8], reproductive toxicity [7], hepatotoxicity [9], and genotoxicity [10] in mammals.

Relevant studies have demonstrated the limited removal efficiency of NEOs in conventional sewage treatment units, resulting in high detection frequencies and concentrations of NEOs in effluent water. For instance, the average concentration of imidacloprid in the effluent from five sewage treatment plants in Beijing ranged from 45 ng/L to 106 ng/L [11]. The average concentrations of clothianidin, imidacloprid and acetamiprid in effluent from 13 wastewater treatment plants in the United States were 70.2 ± 121.8 ng/L, 58.5 ± 29.1 ng/L and 2.3 ± 1.4 ng/L, respectively [12]. Due to the widespread distribution of NEOs in water environment and their ecotoxicological hazards, the removal of residual NEOs in water has become an urgent concern to address. Some studies used efficient NEOs-degrading bacteria for NEOs removal, while the high cultivation costs and operational challenges limited their practical application. The adsorption method, which offers high removal efficiency and relative stability, faces challenges such as competing adsorption of other pollutants and adsorbent regeneration during practical implementation. Membrane treatment technologies require regular cleaning and membrane replacement, which is expensive.

* Corresponding author.
E-mail address: xujian@craes.org.cn (J. Xu).

https://doi.org/10.1016/j.cclet.2023.109413
1001-8417/

Peroxymonosulfate-based advanced oxidation processes (PMS-AOPs) have garnered increasing attention as an effective method for removing refractory organic compounds in water [13,14]. The activation of PMS by transition metals, such as Fe, Co, Mn, Ni, and Cu, has been extensively investigated due to their low energy requirement and high efficiency [15,16]. By anchoring individual metal atoms on the substrate, single-atom catalysts (SACs) maximize exposure to the reactants and provide a family of well-defined molecular structures for mechanistic studies [17]. The abundance of carbon and nitrogen sources has led to a rapid growth of carbon-based SACs with nitrogen coordination, making them a prominent research focus [16,18].

The sulfate radical ($SO_4^{\bullet-}$) has a redox potential of $E^0(SO_4^{\bullet-}/SO_4^{2-}) = +2.60 \sim +3.10$ V_{NHE} at 20 °C and a longer lifetime (30–40 µs) [19] compared to hydroxy radical ($^{\bullet}OH$), which has a lower redox potential of $E^0(^{\bullet}OH/OH^-) = +1.90 \sim +2.70$ V_{NHE} at 20 °C and shorter lifetime (<1 µs). PMS–AOPs have a significantly wider pH application range than most of traditional hydroxyl radical based AOPs [20–22]. Recently, there has been significant interest in designing and preparing efficient catalysts for PMS activation to generate singlet oxygen ($^1O_2$) [23,24]. Because $^1O_2$ is regarded as an effective means of selectively removing contaminants, nonradical-dominated systems offer advantages in terms of adaptability to different pH environments (acidic/neutral/alkaline), resistance to ubiquitous inorganic ions, selectivity for organic contaminants, and moderate redox potential [25,26]. However, the redox potential of singlet oxygen (0.81 V *vs.* NHE) is much lower than that of common radicals ($SO_4^{\bullet-}$: 2.5–3.1 V *vs.* NHE, $^{\bullet}OH$: 1.9–2.7 V *vs.* NHE). The application of nonradical oxidation processes is limited by their low mineralization performance [27]. Considering the characteristics of ROS, a rational catalyst design has the potential to stimulate a synergistic system of radicals and nonradicals, facilitating the more complete removal of target pollutants [28]. To the best of our knowledge, there is a lack of studies on the degradation of NEOs in PMS-AOPs through various oxidation pathways. Therefore, comprehensive experimental investigations are needed to determine whether the synergistic system exhibits superior removal and mineralization performance for refractory pollutants.

This study aims to investigate the effect of different oxidation pathways on the degradation of various NEOs. The functional characteristics of different oxidation pathways and the decomposition properties of NEOs would be analyzed. Heterogeneous PMS activation systems using manganese catalyst (Mn NC) and cobalt catalyst (Co NC) were established to trigger the nonradical oxidation and synergistic oxidation pathway, respectively. Seven representative NEOs with diverse molecular structures (Fig. 1) were selected to examine their decomposition characteristics in the PMS system. The degradation rates and mineralization performance of NEOs in different oxidation systems were measured, and a comparative analysis was conducted to determine the degradation superiority of the nonradical system. Density functional theory (DFT) calculations were used to analyze the differences in charge distribution and reaction sites of various NEOs, providing insights into the influence mechanism of molecular structure on the degradation.

The seven NEOs were obtained from Alta Scientific Co, Ltd. (Tianjin, China). Peroxymonosulfate (PMS, $KHSO_5 \cdot 0.5KHSO_4 \cdot 0.5K_2SO_4$) was purchased from Aladdin Chemistry Co., Ltd. The catalyst synthesis procedure was illustrated in Fig. 2a and described in Text S1 (Supporting information). The electron paramagnetic resonance spectrometer (EPR) and total organic carbon (TOC) detection methods were provided in Text S2 (Supporting information). The concentrations and degradation products of NEOs were determined by ultra-performance liquid chromatography tandem mass spectrometry (UPLC-MS/MS), and the specific conditions are outlined in Text S3 (Supporting information).

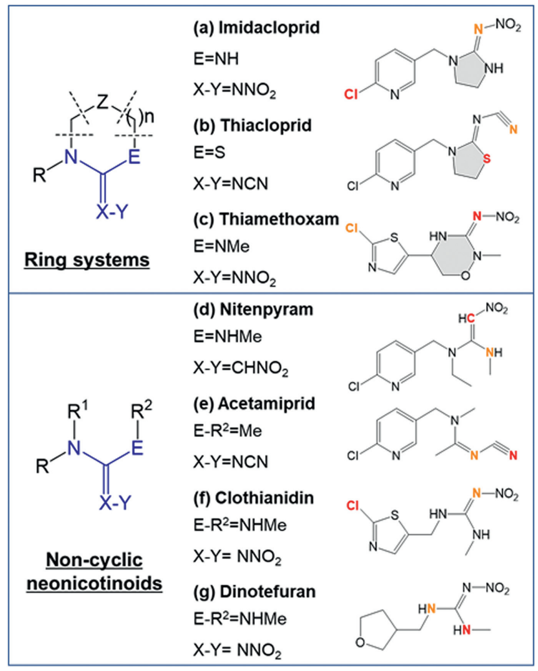

Fig. 1. The selected NEOs: (a–c) ring systems and (d–g) noncyclic NEOs.

The details of the calculation method of *pseudo*-first-order kinetic rate constant (k_{obs}) was given in Text S4 (Supporting information). DFT calculation was employed in this study to elucidate the reactive sites of NEOs, as described in Text S5 (Supporting information).

Uniformly star-like hybrid ZIF catalysts were fabricated as an advanced precursor, as depicted in Fig. 2a. Upon pyrolysis at 910 °C under an N_2 atmosphere, the hybrid ZIF catalysts were transformed into nitrogen-doped porous carbon, as confirmed by X-ray diffraction (XRD) analysis (Fig. 2b) and X-ray photoelectron spectroscopy (XPS) analysis (Fig. 2c). The catalysts retained their initial nanostructure of a regular star shape with six equal branches after pyrolysis (Fig. 2a), while the surface became rougher. The XRD patterns depicted that both Mn NC and Co NC showed broad and weak diffraction at around 25° and 43°, corresponding to the (002) and (101) planes of graphitic carbon (Fig. 2b). No peaks of metal nanoparticles or oxides were detected in the XRD spectra of Mn NC and Co NC, indicating that the metal species were dispersed at the atomic scale. The high-angle annular dark field scanning transmission electron microscopy exhibited independent and dispersed bright sites, further confirming the atomic distribution of the Mn and Co site in Mn NC and Co NC, respectively (Fig. S1 in Supporitng information). XPS spectra exhibited that peaks at 285 eV, 401 eV, and 533 eV were attributed to C 1s, N 1s, and O 1s, respectively. The characteristic peaks at 689 eV and 780 eV confirmed the presence of Mn and Co. The metal content of Mn NC and Co NC was detected by ICP-MS as 1.71% and 1.47%, respectively. The catalysts exhibited similar physical and chemical properties, except for variations in metal type, including morphology, metal content, and carbon substrate characteristics.

PMS activation typically proceeds through radical pathways involving $^{\bullet}OH$ and $SO_4^{\bullet-}$, as well as nonradical pathways involving $^1O_2$. EPR was applied to further identify ROS during the reaction process. As a typical spin capture agent, 5,5-dimethyl-1-pyrroline *N*-oxide (DMPO) was used to confirm the presence of $^{\bullet}OH$ and $SO_4^{\bullet-}$. In the heterogeneous Co NC/PMS system, four strong signals with an intensity ratio of 1:2:2:1 were observed in the EPR spectrum (Fig. 2d), indicating the presence of $^{\bullet}OH$. The six

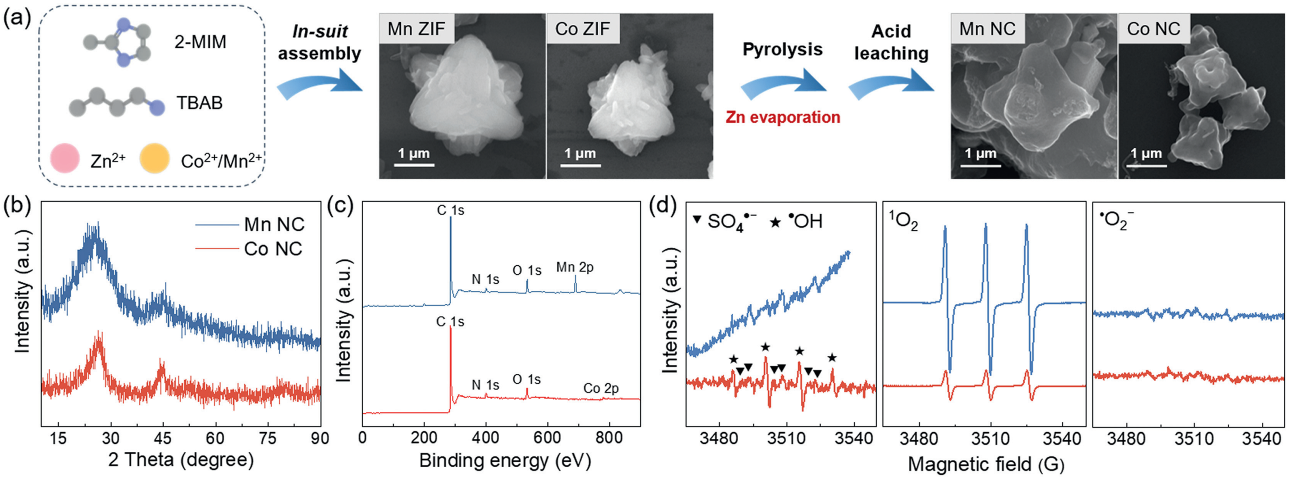

Fig. 2. (a) Schematic illustration of the synthesis process of catalysts; (b) XRD and (c) XPS spectra of catalysts; (d) EPR spectra of Mn NC and Co NC heterogeneous PMS systems.

small peaks around the four strong signals indicated the generation of $SO_4{\bullet}^-$ [29,30]. The seven−line spectrum in the EPR spectra of Mn NC/PMS was attributed to 5,5-dimethyl-1-pyrrolidone-2-oxyl ($DMPO_X$), which was the direct oxidation product of DMPO *via* a nonradical pathway [31]. 2,2,6,6-Tetramethyl-4-piperidinol (TEMP) was used as a capture agent for $^1O_2$. The characteristic signal with an intensity ratio of 1:1:1 was observed in both Co NC/PMS and Mn NC/PMS systems, confirming the presence of $^1O_2$. EPR analysis revealed no signals corresponding to superoxide radical ($^{\bullet}O_2{}^-$) in the Co NC/PMS or Mn NC/PMS system. The heterogeneous PMS activation systems using Mn NC and Co NC triggered the nonradical oxidation pathway and synergistic oxidation pathway, respectively.

NEOs are synthetic compounds with a structure similar to nicotine (Fig. S2 in Supporting information), which exhibit a common mode of action by affecting the central nervous system of insects through binding to nicotinic acetylcholine receptors, making them effective against a wide range of insects. These compounds have low vapor pressure (<0.002 MPa, 25 °C), indicating limited potential for volatilization. They also possess high water solubility (185–590,000 mg/L, 20 °C), low sediment adsorption properties (logK_{oc}: 1.41–3.67), and are resistant to hydrolysis under neutral or acidic pH conditions. Specific physicochemical properties of NEOs are summarized in Table 1. The degradation time of nitro-substituted NEOs (thiamethoxam, clothianidin, and imidacloprid) was 1–2 orders of magnitude shorter than that of cyano−substituted NEOs (acetamiprid and thiacloprid). Notably, the molecular structure of thiacloprid contains a thiophene S site. The electronegativity of the S atom (2.58) is similar to that of the C atom, enabling the generation of spin charges in the carbon lattice [32]. The presence of thiophene S sites in thiacloprid molecules may activate PMS through a synergistic effect of the N configuration [33]. It is predicted that thiacloprid can be rapidly and efficiently degraded in the heterogeneous PMS system.

The energy of the highest occupied molecular orbital (HOMO) indicates the electrophilic reactivity, while the energy gap between the HOMO and the lowest unoccupied molecular orbital (LUMO) serves as an important stability indicator. Table 2 reveals significant differences in HOMO and LUMO distributions among the selected NEOs. NEOs can be classified based on the [−N−C(E)=X−Y] (Fig. 1 and Fig. S2 in Supporitng information), including *N*-cyanoamidines (acetamiprid and thiacloprid), nitromethylene (nitenpyram), and nitroguanidines (dinotefuran, clothianidin, imidacloprid, and thiamethoxam). As shown in Table 2, a uniform electron distribution in the cyano portions of the molecule was observed in the HOMO of acetamiprid and thiacloprid. For nitenpyram, the HOMO distribution shifted towards the nitro-methylene moiety. In the nitroguanidines NEOs, the HOMO distribution was mainly concentrated on the nitroguanidine group, indicating the electron-withdrawing region of the molecular structure. The distribution of electrostatic potential (ESP) with an isosurface of 0.2 (blue and red representing positive and negative values, respectively) in Table 2 was calculated to predict reactive sites. The ESP analysis, consistent with the HOMO analysis, revealed that the specific substituents (highlighted in red) involved atoms that were prone to undergo electrophilic reactions. The differences in molecular reactivity and product distribution primarily stemmed from the variations in the =X–Y. Y refers to the nitro group ($-NO_2$) and cyanide group (−C≡N), both of which are strong electron−withdrawing groups with conjugation and induction effect, causing a shift in the electron cloud distribution within the molecular structure and a reduction in electron density. These structural characteristics make the corresponding regions more susceptible to be attacked by negatively charged radicals, thereby increasing the reaction activity. According to the frontier molecular orbital (FMO) theory, ΔE is an important stability indicator that can help to explain the activity and stability of the molecule. A smaller ΔE value indicates a more reactive molecule. Table 2 summarizes the ΔE energies of seven NEOs. Apart from thiacloprid, acetamidine exhibits the largest ΔE, while nitenpyram has the smallest ΔE. Nitenpyram is predicted to undergo the fastest degradation, while acetamiprid is expected to degrade the slowest.

The Fukui function (f) calculation method has been employed to predict the potential active sites of NEOs in oxidative decomposition reactions, providing insights into the analysis of degradation products. Atoms with high f^- values in NEOs molecules are more prone to electron loss and oxidation through electrophilic attacks, while atoms with high f^0 values are more susceptible to radical attacks. The optimized molecular structures and calculated charge distributions of the seven NEOs are depicted in Fig. 3. The atomic sites highlighted in red and orange in the molecular structure diagrams of NEOs (Table 1 and Fig. 1) represented atomic sites with high f^- and f^0 values, respectively. These atomic sites were vulnerable to be attacked during the oxidation process.

The heterogeneous PMS activation system by Mn NC and Co NC to trigger nonradical oxidation and synergistic oxidation pathways are shown in Fig. 4. It demonstrated significant differences in the degradation efficiency of NEOs (ranging from 49.3% to 99.7%) within 60 min. The reaction kinetics of NEOs analyzed by the

Table 1
Structures and properties of seven NEOs.

NEOs	Imidacloprid	Thiacloprid	Thiamethoxam	Nitenpyram	Acetamiprid	Clothianidin	Dinotefuran
Molecule	$C_9H_{10}ClN_5O_2$	$C_{10}H_9ClN_4S$	$C_8H_{10}ClN_5O_3S$	$C_{11}H_{15}ClN_4O_2$	$C_{10}H_{11}ClN_4$	$C_6H_8ClN_5O_2S$	$C_7H_{14}N_4O_3$
Structure	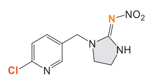	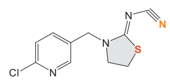	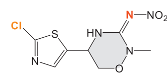	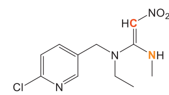	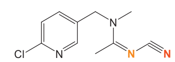	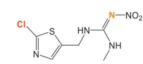	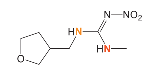
pK_a	7.16 ± 0.20	0.01 ± 0.10	0.99 ± 0.10	2.46 ± 0.70	−0.44 ± 0.10	2.76 ± 0.50	3.24 ± 0.50
Water solubility (at 20 °C, g/L)	0.610	0.185	4.100, at 25 °C	>570.000	4.250, at 25 °C	0.327	54.300 ± 1.300
Molecule weight (g/mol)	255.7	252.7	291.7	270.7	222.7	249.7	202.2
Vapor pressure (20 °C, MPa)	4.0×10^{-7}	3.0×10^{-7}	6.6×10^{-6}	1.1×10^{-3}	1.7×10^{-4}	2.8×10^{-8}	1.7×10^{-3}
Density (20 °C, g/mL)	1.54	1.46	1.57	1.40 (at 26 °C)	1.33	1.61	1.33
Melting point (°C)	144	136	139	83–84	98.9	176.8	94.6–101.5
Lipophilicity (log$P_{o/w}$)	0.57 at 22 °C	1.26 at 20 °C	−0.13 at 25 °C	−0.64 at 25 °C	0.8 at 25 °C	0.7 at 25 °C	0.644 at 25 °C
Soil affinity (logK_{oc})	2.19–2.90	3.67	1.75	1.78	2.3	2.08	1.41
Water hydrolysis (DT_{50} in days)	Stable > 1 year (pH 9)	Stable	Stable 11.5 (pH 9)	Stable 2.9 (pH 9)	Stable 420 (pH 9)	Stable 14.4 (pH 9)	Stable

Table 2
The HOMO and LUMO distribution of NEOs.

NEOs	Imidacloprid	Thiacloprid	Thiamethoxam	Nitenpyram	Acetamiprid	Clothianidin	Dinotefuran
LUMO	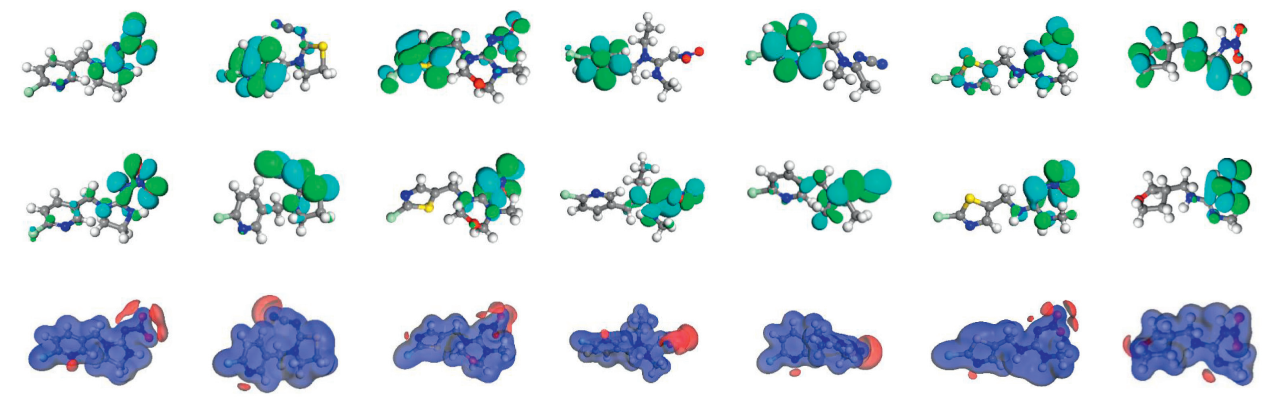						
HOMO							
ESP							
E_{HOMO} (eV)	−5.831	−6.396	−5.765	−5.346	−6.603	−5.766	−5.968
E_{LUMO} (eV)	−1.827	−2.222	−1.914	−2.485	−2.472	−1.847	−2.577
ΔE (eV)	4.004	4.174	3.851	2.861	4.131	3.919	3.391

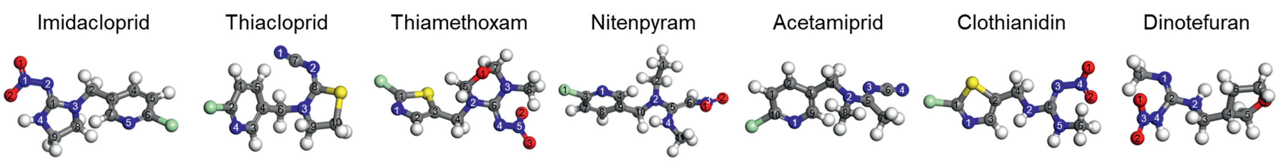

Imidacloprid

	No	f^-	f^0
C	1	0.029	0.043
C	2	-0.019	-0.017
C	3	0.004	-0.005
C	4	0.007	0.035
C	5	0.023	0.029
C	6	0.014	0.011
C	7	0.014	0.027
C	8	-0.023	-0.021
C	9	-0.016	-0.015
O	1	0.167	0.154
O	2	0.173	0.145
N	1	0.030	0.046
N	2	0.071	0.048
N	3	0.040	0.023
N	4	0.023	0.024
N	5	0.033	0.050
Cl	1	0.095	0.087

Thiacloprid

	No	f^-	f^0
C	1	0.018	0.026
C	2	0.011	0.025
C	3	0.013	0.031
C	4	-0.003	0.004
C	5	-0.007	0.0515
C	6	-0.023	-0.017
C	7	0.087	0.046
C	8	0.002	0.012
C	9	-0.029	-0.023
C	10	-0.02	-0.016
N	1	0.182	0.121
N	2	0.129	0.087
N	3	0.054	0.026
N	4	0.035	0.071
Cl		0.079	0.100
S		0.193	0.140

Thiamethoxam

	No	f^-	f^0
C	1	0.019	0.046
C	2	0.03	0.03
C	3	-0.009	0.018
C	4	-0.023	-0.0195
C	5	-0.021	-0.0155
C	6	0.023	0.0305
C	7	-0.017	-0.0135
C	8	-0.028	-0.0255
O	1	0.182	0.148
O	2	0.187	0.141
O	3	0.027	0.024
N	1	0.029	0.044
N	2	0.033	0.014
N	3	0.030	0.021
N	4	0.099	0.058
N	5	0.027	0.036
Cl		0.073	0.0925
S		0.027	0.0795

Nitenpyram

	No	f^-	f^0
C	1	-0.014	-0.009
C	2	-0.045	-0.032
C	3	0.005	0.009
C	4	0.000	0.032
C	5	0.019	0.022
C	6	0.158	0.083
C	7	0.012	0.032
C	8	0.002	0.059
C	9	-0.019	-0.014
C	10	-0.017	-0.015
C	11	-0.038	-0.028
N	1	0.015	0.064
N	2	0.005	-0.005
N	3	0.006	0.014
N	4	0.050	0.027
O	1	0.165	0.120
O	2	0.134	0.095
Cl		0.045	0.077

Acetamiprid

	No	f^-	f^0
C	1	0.019	0.0405
C	2	0.007	0.070
C	3	-0.010	-0.0065
C	4	-0.030	-0.0215
C	5	0.021	0.017
C	6	0.105	0.055
C	7	-0.017	-0.013
C	8	-0.040	-0.0285
C	9	0.004	0.032
C	10	0.010	0.013
N	1	0.025	0.077
N	2	0.101	0.043
N	3	0.125	0.0625
N	4	0.201	0.1365
Cl		0.074	0.0995

Clothianidin

	No	f^-	f^0
C	1	0.029	0.043
C	2	0.016	0.023
C	3	0.039	0.033
C	4	-0.024	-0.024
C	5	0.021	0.032
C	6	-0.029	-0.030
N	1	0.034	0.040
N	2	0.019	0.012
N	3	0.075	0.051
N	4	0.023	0.044
N	5	0.044	0.033
O	1	0.154	0.140
O	2	0.156	0.152
Cl		0.105	0.100
S		0.078	0.097

Dinotefuran

	No	f^-	f^0
C	1	-0.040	-0.041
C	2	0.024	-0.002
C	3	-0.039	-0.035
C	4	-0.023	-0.016
C	5	-0.030	-0.016
C	6	-0.018	-0.013
C	7	-0.039	-0.023
N	1	0.120	0.100
N	2	0.104	0.063
N	3	0.000	0.067
N	4	0.001	0.040
O	1	0.059	0.155
O	2	0.021	0.135
O	3	0.147	0.082

Fig. 3. The molecular structure and Fukui index of NEOs.

pseudo-first-order reaction model (Fig. S3 in Supporitng information) followed the order of $k_{thiacloprid}$ (0.1014 min^{-1}) > $k_{nitenpyram}$ (0.0409 min^{-1}) > $k_{dinotefuran}$ (0.0387 min^{-1}) > $k_{imidacloprid}$ (0.0331 min^{-1}) > $k_{thiamethoxam}$ (0.0255 min^{-1}) > $k_{clothianidin}$ (0.0234 min^{-1}) > $k_{acetamiprid}$ (0.0128 min^{-1}). The selective oxidation of NEOs in the Mn NC/PMS nonradical system was illustrated in Fig. 4b, indicating different degradation capabilities of NEOs. The complete removal of imidacloprid, thiacloprid, and clothianidin was achieved. Except for dinotefuran, the degradation rates of the other six NEOs were higher than those in the single oxidation process, with $k_{dinotefuran}$ decreasing from 0.0876 min^{-1} to 0.0387 min^{-1}. It was likely attributed to the PMS activation capability of thiophene S in thiacloprid. Not only the regulation of ROS can affect pollutant removal, but also the coexistence of similar substances can significantly impact subsequent degradation. Different ROS selectively targeted specific sites in organic compounds, allowing for the production of low−toxicity oxidation products through reasonable ROS regulation. Instead of solely mineralizing pollutants, converting them into more valuable addition polymers may be conducive to achieving carbon peaking and neutrality [34]. The production of addition polymers should be taken into account.

Considering the characteristics of ROS, rational catalyst design has the potential to stimulate a synergistic system of radicals and nonradicals, leading to more thorough removal of target contaminants. Figs. 4c and d illustrates the degradation performance of NEOs in the Co NC/PMS system, which involves $^{\bullet}OH$, $SO_4^{\bullet-}$, and $^1O_2$. As seen from Fig. 4c, thiamethoxam, clothianidin, and acetamiprid cannot be effectively degraded in the heterogeneous Co NC/PMS oxidation system, with removal efficiencies of only 14.9%, 17.5%, and 38.1%, respectively. These values were significantly lower than those achieved in the nonradical process using Mn NC/PMS. Conversely, imidacloprid, thiacloprid, and nitenpyram exhibited re-

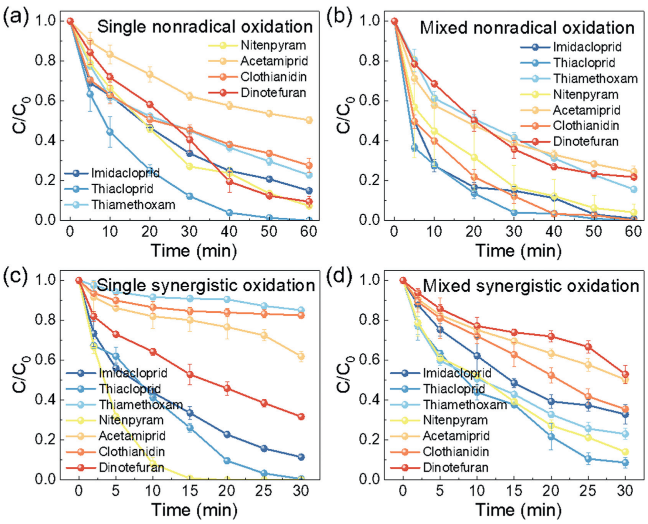

Fig. 4. (a) NEOs degradation performances in single nonradical oxidation system (Experimental conditions: Mn NC dosage = 0.05 g/L, $[PMS]_0$ = 0.75 mmol/L, [Single NEOs] = 1 ppm, unadjusted pH, and T = 25 °C); (b) NEOs degradation performances in mixed nonradical oxidation system (Experimental conditions: Mn NC dosage = 0.05 g/L, $[PMS]_0$ = 0.75 mmol/L, [Mixed NEOs, the concentration of each compound is 0.14 ppm] = 1 ppm, unadjusted pH, and T = 25 °C); (c) NEOs degradation performances in single synergistic oxidation system (Experimental conditions: Co NC dosage = 0.05 g/L, $[PMS]_0$ = 0.75 mmol/L, [Single NEOs] = 1 ppm, unadjusted pH, and T = 25 °C); (d) NEOs degradation performances in mixed synergistic oxidation system (Experimental conditions: Co NC dosage = 0.05 g/L, $[PMS]_0$ = 0.75 mmol/L, [Mixed NEOs, the concentration of each compound is 0.14 ppm] = 1 ppm, unadjusted pH, and T = 25 °C).

markably high removal efficiencies, with degradation rates as high as 0.0742, 0.1430 and 0.3007 min^{-1}, respectively (Figs. S4a and b in Supporting information), much higher than those in the Mn NC/PMS nonradical oxidation processes. However, in the mixed reaction process involving multiple NEOs (Fig. 4d, Figs. S4c and d in Supporting information), the removal efficiency (from 47.0% to 91.3%) and rate (from 0.0192 min^{-1} to 0.0816 min^{-1}) differed significantly from those observed in the single oxidation system. The degradation efficiency of thiamethoxam and clothianidin was greatly improved, reaching 77.0% and 64.5%, respectively. Notably, the degradation rate of thiamethoxam increased by 9.5 times. However, the k_{obs} values of nitenpyram and dinotefuran sharply decreased by 78.52% and 50.77%, respectively. These results highlighted the need to optimize both the composition of ROS in persulfate-AOPs and the contaminant components and their properties for effective wastewater purification.

The degradation efficiency of thiacloprid reached 100% after 60 min and 30 min in the nonradical oxidation and synergistic oxidation system, respectively. Fig. 5 demonstrates that the corresponding mineralization efficiencies were 57.3% and 60.4%, respectively. When complete transformation of the pollutant was achieved, the mineralization performances of the nonradical oxidation and synergistic oxidation systems were similar. Similar trends were observed in the degradation reactions of imidacloprid, nitenpyram, and acetamiprid. The mineralization efficiency of pollutants in the nonradical oxidation system was higher than that in the synergistic oxidation system. Conversely, the removal efficiency of dinotefuran in the nonradical oxidation and synergistic oxidation systems was 90.5% and 68.3%, respectively. The synergistic oxidation system exhibited higher mineralization capability for pollutants. It has been reported that strong oxidation by radicals ($^{\bullet}OH$ and $SO_4^{\bullet-}$) achieved high mineralization of refractory organic pollutants, while the mineralization ability of $^1O_2$ under the same experimental conditions was weaker [35,36]. Considering the experimental results in this study, it is evident that not only the oxidation capacity of ROS but also the nature of the specific target

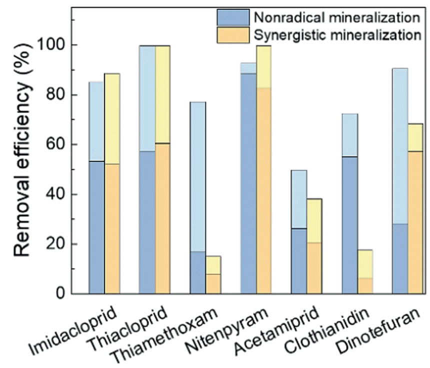

Fig. 5. The removal efficiency and mineralization of NEOs degradation in heterogeneous PMS system (Experimental conditions: Catalyst dosage = 0.05 g/L, $[PMS]_0$ = 0.75 mmol/L, [Single NEOs] = 1 ppm, unadjusted pH, and T = 25 °C).

pollutant needed to be considered when predicting the degree of pollutant mineralization in the oxidation system.

The degradation of NEOs varied greatly, and the four non-cyclic NEOs exhibited distinct degradation characteristics. The ring structure of NEOs was not directly correlated with their decomposition properties in nonradical and synergistic oxidation processes. For instance, both imidacloprid and thiamethoxam were nitroguanidines with a ring structure, yet there was a noticeable difference in their k_{obs} values, indicating that the same structure of [−N−C(E)=X−Y] cannot be directly linked to the decomposition of NEOs. Fig. S6 (Supporting information) illustrates that the selective removal of pollutants in heterogeneous persulfate system cannot be solely based on a specific physicochemical property of the pollutants.

There were significant differences in the distribution of HOMO and LUMO among NEOs, as discussed in above section and listed in Table 2. A higher E_{HOMO} indicates greater electrophilic activity of the organic molecule. The conversion rate of the target contaminant in the oxidation reaction should be proportional to the value of E_{HOMO} and inversely proportional to ΔE. As shown in Fig. 6, for the seven selected NEOs, the degradation regularities were observed in both nonradical oxidation and synergistic oxidation processes. Notably, the concentration of each NEOs was 1 ppm, for a total of 7 ppm in the mixed degradation process, labeled as "Mixed nonradical oxidation II" and "Mixed synergistic oxidation II" (Fig. 6). The relationship between E_{HOMO} and k_{obs} did not exhibit a strong linear correlation. The differences in the energy gap of NEOs cannot be solely attributed to a single substituent or the changes in the distribution of HOMO. The number of active sites in these NEOs molecules varied, leading to differences in the energy gap. Thiacloprid, due to the presence of specific thiophene S, acted not only as a degrading pollutant but also as a persulfate activator. Except thiacloprid, the degradation rate of NEOs was inversely proportional to ΔE. The differences in ΔE among NEOs can be attributed to changes in HOMO and LUMO distributions caused by different substituents. For instance, nitro group ($-NO_2$) and cyanide group (−C≡N), which have conjugation and inductive effects, could shift the electron cloud distribution of the molecular structure. Compounds with electron donor substituents were more easily oxidized than those with electron-withdrawing substituents. Therefore, the type and number of substituents can affect the electron distribution and activity of NEOs molecules, resulting in differences in the degradation rate during the oxidation reaction.

The electron-rich sites on NEOs are the active sites that may be attacked in the Mn-NC/PMS system. In the Co-NC/PMS system, there are both radicals and nonradicals, and the active sites on NEOs that may be attacked include atomic sites with high f^- and

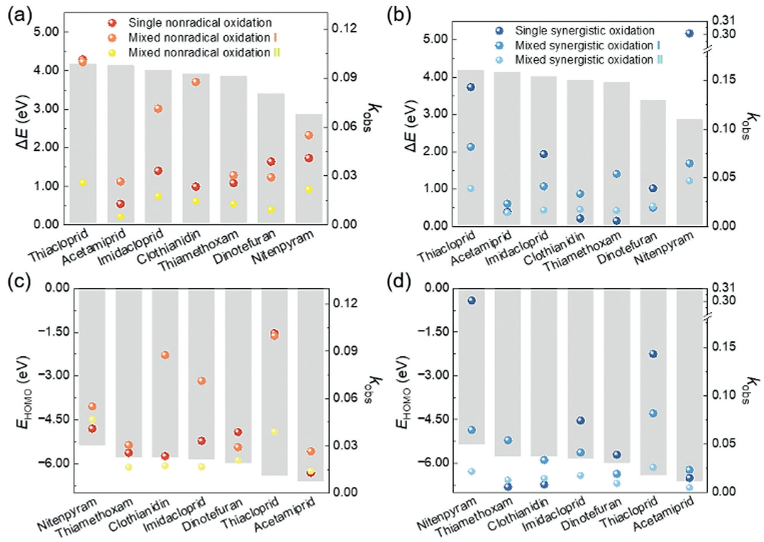

Fig. 6. Correlation of k_{obs} to E_{HOMO} and ΔE.

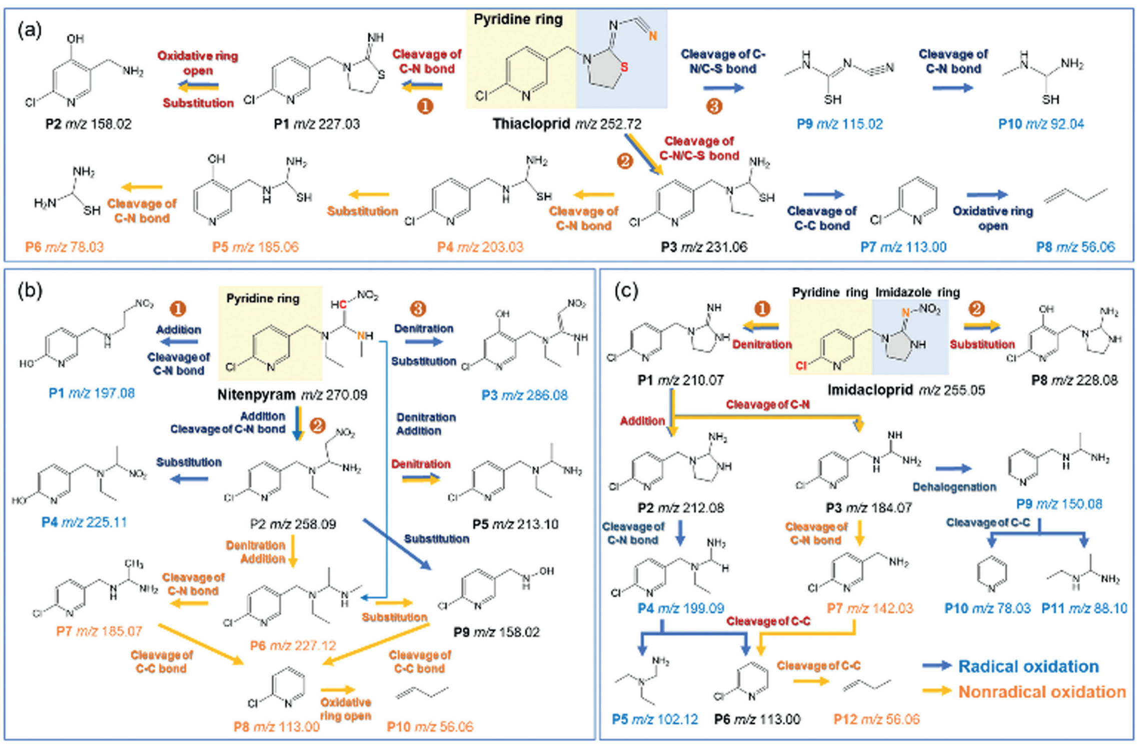

Fig. 7. Representative degradation pathways of (a) *N*–cyanoamidine (thiacloprid), (b) nitromethylene (nitenpyram), and (c) nitroguanidine (imidacloprid) NEOs.

f^0. As seen from Table 2, the HOMO of the seven NEOs was located at [−N−C(E)=X−Y], particularly at the =X-Y position, highlighting the site where electrons were easily released. Fig. 3 further identifies that the N atom in the =X-Y structure of the selected NEOs was the active site on NEOs that may be susceptible to be attacked during PMS oxidation. The oxidation products were subsequently determined using UPLC−MS/MS. Thiacloprid, nitenpyram, and imidacloprid all contain pyridine rings in their molecular structures and belong to the *N*-cyanoamidine, nitromethylene, and nitroguanidine NEOs, respectively. These three NEOs were selected as representative compounds based on the classification of [−N−C(E)=X−Y] to analyze the possible degradation products (Tables S2–S4 in Supporting information) and decomposition pathways (Fig. 7).

Nitro group (−NO_2) and cyanide group (−C≡N) are strong electron-withdrawing groups that exhibit conjugation and induction effects. These characteristics resulted in a shift in the electron cloud at the C or N sites adjacent to the *Y* structure, leading to a reduction in electron density. Such molecular structure characteristics made these regions more susceptible to be attacked by negatively charged radicals, thereby increasing the reaction activity. Specifically, the N atoms in NEOs molecules, including N3 and N4 in imidacloprid, N2 and N3 in thiacloprid, and N4 in nitenpyram, possess strong electronegativity. The charge on these N atoms was higher than the average charge of the entire NEOs molecule, and they contained a greater number of electrons, making them more susceptible to radical attack. It is important to note that while the Fukui function calculation values for N, O, and C in −NO_2 and

–C≡N were high, these functional groups were considered as a whole substituent, and the individual atomic sites cannot participate in the reaction alone.

The initial reaction of the dominant ROS species with NEOs would significantly impact the subsequent reactions. The distribution of HOMO, LUMO and ESP in the dominant ROS was calculated to analyze the NEOs degradation process (Table S4 in Supporting information). The blue and red surfaces in the ESP represented positive and negative values, respectively. The ESP directly showed that $^{\bullet}OH$ surface exhibited a symmetrical positive and negative charge distribution, making it highly reactive towards most organic pollutants. The static charges on the surface of $SO_4^{\bullet-}$ and $^1O_2$ were mainly negative and positive, respectively. $SO_4^{\bullet-}$ was more inclined to attack electron donor groups, and would transform NEOs through electrophilic/radical addition and electron transfer to break bonds. The surface static charge of $^1O_2$ was almost entirely positive. $^1O_2$ is selective to electron-rich substituents, leading to C–N/C–S bond breakage and other reactions.

The induced effect shifted the electron cloud on the C=N to the cyanide group (–C≡N), making the addition reaction more likely to occur on the C=N bond (degradation path 1 and 2 in Fig. 7a). The degradation of thiacloprid was initiated with the cleavage of the C7–N2 bond at the C7 ($f^- = 0.087$, $f^0 = 0.046$) through an attack by electrophilic species, resulting in the formation of **P1**. As presented in Fig. 3, the C5 atom ($f^0 = 0.052$) on the pyridine ring of thiacloprid exhibited high reactivity with $^{\bullet}OH$ and $SO_4^{\bullet-}$. The Cl atom ($f^- = 0.079$, $f^0 = 0.100$), with high Fukui function calculation value, presented high reactivity with $^1O_2$, $^{\bullet}OH$ and $SO_4^{\bullet-}$, leading to oxidative ring open and substitution reaction generating **P2**. Thiacloprid could also be transformed into **P3**, facilitated by the high electron cloud density of the thiophene S. Subsequently, **P3** could transform into **P4** through the breakage of a C–N bond due to $^1O_2$ oxidation. The substitution reaction resulted in the formation of **P5**, followed by the cleavage of the C–N bond to produce **P6**. **P3** could also be converted to **P7** *via* the strong oxidation of $^{\bullet}OH$ and $SO_4^{\bullet-}$, further generating a small molecule organic matter **P8**. $^{\bullet}OH$ and $SO_4^{\bullet-}$ could attack the thiophene ring to break the C–N and C–S bonds, resulting in the formation of **P9** (path 3 in Fig. 7a), followed by the cleavage of C–N to produce **P10**. Similarly, the induced effect shifted the electron cloud on the C=C to the nitro group (–NO_2) in nitenpyram, making the addition reaction more likely to occur on the C=C bond (degradation path 1 and 2 in Fig. 7b). Combined with the cleavage of the C5–N4 and C11–N4 bonds, **P1** and **P2** were generated, respectively. The hydroxyl radical addition to the C8 atom ($f^0 = 0.059$) on the pyridine ring occurred, generating **P3** in the synergistic oxidation system (degradation path 3 in Fig. 7b). The degradation products of nitenpyram in the nonradical oxidation system and synergistic oxidation system were different. The calculation results of the Fukui function for nitenpyram were shown in Fig. 3, indicating significant differences between the f^- and f^0 values at every possible reactive sites. Based on the structure of organic matter, the oxidative degradation path of NEOs were predicted and determined according to the Fukui function indexes and the properties of ROS. In the degradation process of imidacloprid (Fig. 7c), both of **P1** and **P8** were generated through the denitration reaction, facilitated by the induced effect of the nitro group (–NO_2).

From the degradation path (Fig. 7), the C and N sites adjacent to the nitro group (–NO_2) and cyanide group (–C≡N) were more susceptible to oxidation attacks. The initial stages of degradation for the three typical NEOs mainly involved C–N/C–C bond breaking reactions and C=C/C=N additions. And the S and N atoms, which possess strong electronegativity and high electron cloud density, were also key active sites in the degradation pathway. The degradation process often involved substitution reactions on the pyridine ring, where $^{\bullet}OH$ replaced H or Cl atoms. The sites of substitution reactions were influenced by the substituent groups on the pyridine ring, which was estimated using the Fukui function calculations.

This study established the heterogeneous PMS activation systems by Mn NC and Co NC to trigger nonradical oxidation pathway and synergistic oxidation pathway, respectively. The synergistic oxidation system exhibited lower degradation and mineralization efficiency of NEOs compared to nonradical oxidation. The composition of organic pollutants in wastewater was crucial as it can significantly impact degradation processes. Combining DFT calculations, it showed that the reactivity of various refractory pollutants with different structures in the oxidation system could be directly predicted using ΔE, which served as a reliable indicator for assessing pollutant reactivity. Concisely deduced degradation pathways of different NEOs provided valuable insights into the impact of different substituents on the degradation of NEOs. It was demonstrated that the C and N sites adjacent to the nitro group and cyanide group were more susceptible to oxidation attacks. Additionally, S and N atoms, which possess strong electronegativity and high electron cloud density, were identified as key active sites in the degradation pathway.

Declaration of competing interest

The authors declare that they have no known competing financial interests or personal relationships that could have appeared to influence the work reported in this paper.

Acknowledgment

This work was funded by National Natural Science Foundation of China (No. 42177382).

Supplementary materials

Supplementary material associated with this article can be found, in the online version, at doi:10.1016/j.cclet.2023.109413.

References

[1] P. Jeschke, R. Nauen, M. Schindler, et al., J. Agric. Food Chem. 59 (2011) 2897–2908.
[2] X. Shao, Z. Liu, X. Xu, et al., J. Pestic. Sci. 38 (2013) 1–9.
[3] M.L. Hladik, A.R. Main, D. Goulson, Environ. Sci. Technol. 52 (2018) 3329–3335.
[4] B.Z. Bradford, A.S. Huseth, R.L. Groves, PLoS One 13 (2018) e0201753.
[5] K.L. Klarich, N.C. Pflug, E.M. DeWald, et al., Environ. Sci. Technol. Lett. 4 (2017) 168–173.
[6] Y. Wan, Y. Wang, W. Xia, et al., Sci. Total Environ. 675 (2019) 513–519.
[7] T. Hirano, S. Yanai, T. Omotehara, et al., J. Vet. Med. Sci. 77 (2015) 1207–1215.
[8] S. Özdemir, S. Altun, M. Özkaraca, et al., Chemosphere 203 (2018) 318–326.
[9] L. Xu, X. Xu, L. Guo, et al., Environ. Sci. Technol. 55 (2021) 7541–7550.
[10] P.D. Stivaktakis, M.P. Kavvalakis, M.N. Tzatzarakis, et al., Chemosphere 149 (2016) 108–113.
[11] W. Qi, H. Singer, M. Berg, et al., Chemosphere 119 (2015) 1054–1061.
[12] A.M. Sadaria, S.D. Supowit, R.U. Halden, Environ. Sci. Technol. 50 (2016) 6199–6206.
[13] W.D. Oh, Z. Dong, T.T. Lim, Appl. Catal. B: Environ. 194 (2016) 169–201.
[14] C. Chen, H. Feng, Y. Deng, Water Res. 153 (2019) 100–107.
[15] M. Yang, Z. Hou, X. Zhang, et al., Environ. Sci. Technol. 56 (2022) 11635–11645.
[16] X. Song, Y. Shi, Z. Wu, et al., Appl. Catal. B: Environ. 340 (2024) 123240.
[17] Y. Shang, Y. Kan, X. Xu, Chin. Chem. Lett. 34 (2023) 108278.
[18] Q. Yin, H. Yan, Y. Liang, et al., Sep. Purif. 318 (2023) 123970.
[19] X. Li, X. Huang, S. Xi, et al., J. Am. Chem. Soc. 140 (2018) 12469–12475.
[20] X. Wu, J.H. Kim, ACS ES&T Eng. 2 (2022) 1776–1796.
[21] S. Giannakis, K.Y.A. Lin, F. Ghanbari, Chem. Eng. J. 406 (2021) 127083.
[22] R. Guo, B. Xi, C. Guo, et al., Environ. Funct. Mater. 1 (2022) 239–252.
[23] X. Mi, P. Wang, S. Xu, et al., Angew. Chem. Int. Ed. 133 (2020) 4638–4643.
[24] L.S. Zhang, X.H. Jiang, Z.A. Zhong, et al., Angew. Chem. Int. Ed. 60 (2021) 21751–21755.
[25] Y. Zhou, J. Jiang, Y. Gao, et al., Environ. Sci. Technol. 49 (2015) 12941–12950.
[26] P. Liang, C. Zhang, X. Duan, et al., Environ. Sci. Nano. 4 (2017) 315–324.
[27] X. Duan, H. Sun, Z. Shao, et al., Appl. Catal. B: Environ. 224 (2018) 973–982.

[28] W. Ren, C. Cheng, P. Shao, et al., Environ. Sci. Technol. 56 (2022) 78–97.
[29] Y. Liu, S. Liu, M. Chen, et al., J. Hazard. Mater. (2023) 132417.
[30] L. Lai, H. Zhou, Y. Hong, et al., Chin. Chem. Lett. 35 (2024) 108580.
[31] X. Li, X. Wen, J. Lang, et al., Angew. Chem. Int. Ed. 62 (2023) e202303267.
[32] W. Chen, L. Lei, K. Zhu, et al., J. Environ. Sci. 129 (2023) 213–228.
[33] K. Zhu, Y. Shen, J. Hou, et al., Chem. Eng. J. 412 (2021) 128521.
[34] N. Li, J. Ye, H. Dai, et al., Water Res. 235 (2023) 119926.
[35] T. Wang, J. Zhou, W. Wang, et al., Chin. Chem. Lett. 33 (2022) 2121–2124.
[36] X. Wang, Z. Xiong, H. Shi, et al., Appl. Catal. B: Environ. 329 (2023) 122569.